Proceedings of the ASME 2023 42nd International Conference on Ocean, Offshore and Arctic Engineering
OMAE2023
June 11-16, 2023, Melbourne, Australia

OMAE2023-101302

NUMERICAL ANALYSIS OF FLEXIBLE TUBE WAVE ENERGY CONVERTOR USING CFD-FEA METHOD

Yang Huang[1], Qing Xiao[1]*, Guillermo Idarraga[2], Liu Yang[2], Saishuai Dai[1], Farhad Abad[1], Feargal Brennan[1], Saeid Lotfian[1]
[1]Department of Naval Architecture, Ocean & Marine Engineering, University of Strathclyde, Glasgow, UK
[2] Advanced Composite Group, Department of Mechanical and Aerospace Engineering, University of Strathclyde, Glasgow, UK
*Corresponding author: qing.xiao@strath.ac.uk

ABSTRACT

To better understand the performance of flexible tube wave energy converters (WECs) in ocean waves, a coupled numerical analysis tool based on computational fluid dynamics and a finite element method is employed to perform numerical simulations for the well-known Anaconda WEC under given different regular wave conditions. The nonlinear behaviour of Natural Rubber is considered by using YEOH hyper-elastic model. Fluid-structure interaction responses of the Anaconda WEC are compared considering the impact of incident wave speed on the performance of the device. The free surface around the WEC, internal pressure and velocity in the flexible tube, structure deformation and stress distribution are fully explored. The results show that the proposed numerical analysis tool in this work is able to predict the complex fluid-structure interactions of flexible tube WEC in waves, including wave nonlinearity and inhomogeneous distribution of stress at cross-section. The typical resonant responses are also captured when the incident wave speed matches the bulge wave speed. The internal pressure amplitude, capture width, structural deformation and hoop stress all increase at resonance. Moreover, the deformed shape of the flexible tube is found to depend on the ratio of wavelength to tube length.

Keywords: Flexible wave energy converter, Fluid-structure interaction, Computational fluid dynamics, Finite element analysis, Anaconda WEC.

1. INTRODUCTION

With the development of wave energy converters (WECs), the application of flexible structures in the WECs has recently attracted attention. Various flexible WECs' designs have been proposed to improve the performance in terms of fatigue life, survivability and adaptability of the devices to the dynamic condition of the sea [1]. One of the most widely studied designs is the flexible tube WEC, which has the advantages of lower capital expenditures, easier ramp up in volumes, reduced costs of installation and reduced operating expenses [2]. Compared with conventional point-absorber WEC, it is able to absorb wave energy within a wider range of wave frequencies, indicating that the flexible tube WEC has great potential for the wave energy development. However, it is noted that the fluid-structure interaction of the flexible tube WEC is a rather complex problem, involving the interaction of incident wave and flexible tube, the structure deformation and the coupling of internal flow and external incident wave. Accordingly, most of the existing studies employ some idealised assumptions to simplify this problem. However, in this condition, nonlinear responses, such as wave nonlinearity, are ignored. It is therefore necessary to study the performance of flexible tube WEC in waves for a deeper understanding.

A series of physical model tests have been carried out to explore the performance of flexible tube WEC in various wave conditions. Heller et al. [3] conducted wave tank tests for a 1:25 scale Anaconda WEC model [4], consisting essentially of a closed rubber tube filled with water. They calculated the bulge wave speeds of the flexible tube using measured distensibility based on linear theory [5]. The results agreed with the measured bulge wave speed by means of strain gauges. The capture width (CW) of the Anaconda model was found to be optimal when the bulge wave speed was close to the external wave speed, named the resonant phenomenon. Chaplin et al. [6] carried out a series of wave tank tests for the same Anaconda model with a linear power take-off (PTO) of adjustable impedance. The bulge wave speed was found to decrease with increasing internal pressure. Regardless of the PTO impedance, the CW reached a peak value when the bulge wave speed matched the water wave speed, and the peak value was not much affected by the impedance. While the power curve became narrow as the impedance was increased. Mendes et al. [7] tested a 1:50 scale physical model of a freely floating Anaconda model with an air-flow PTO. The effects of

air compressibility on power generation were discussed in detail. The influence of scale effects on the performance of the Anaconda model was also studied. Moreover, Checkmate Flexible Engineering Ltd. [8] conducted several model tests in order to promote the commercialization of Anaconda WEC. Fixed and freely moving conditions were considered in their tests, and a new PTO was also designed to better capture the wave energy.

In addition to model tests, numerical simulations are also widely used in the research of flexible tube WECs. Due to the complexity of the fluid-structure interaction of flexible tube WEC in waves, idealized assumptions are usually adopted in numerical methods to simplify the problem. For instance, the inner flow in the flexible tube is assumed to be one-dimensional flow and the external wave is assumed to be linear. Moreover, the six-degree-of-freedom (6DoF) motions of the WEC are ignored in existing numerical studies. Based on linear potential flow theory and the one-dimensional (1D) finite element method (FEM), Babarit et al. [9] proposed a linear numerical model for predicting the hyper-elastic responses of the Anaconda WEC. To validate the model, they compared the numerical results with experimental data, showing reasonable agreement between two. This model was later used to estimate the power performance of a prototype device. Chaplin et al. [6, 10, 11] developed a reduced model based on a linear theory to predict the propagation of bulges and power conversion in the Anaconda WEC. The behaviour of WEC predicted by the model was in good agreement with the measured data although the wave nonlinearity induced by wave structure interaction was ignored in their studies.

In this paper, to better understand the nonlinear responses of flexible tube WEC in waves, we employ a coupled analysis model [12] based on computational fluid dynamics (CFD) and finite element analysis (FEA) for the Anaconda WEC. Numerical simulations are performed considering a commercial Natural Rubber material for the flexible tube and regular wave conditions. Fluid-structure interaction responses of the WEC are compared considering the impact of the incident wave speed on the performance of the device. The free surface around the WEC, velocity and pressure variation in the flexible tube, structure deformation, and stress distribution are fully analysed.

2. NUMERICAL ANALYSIS TOOL

To perform fluid-structure interaction (FSI) simulations for the flexible tube WEC, a coupled analysis tool is employed, including a fluid solver, a structure solver and a multi-physical coupling library.

2.1 Fluid solver

A two-phase CFD solver olaFlow [13, 14] developed based on OpenFOAM is used to model the three-dimensional (3D) viscous flow around the WEC. Volume of Fluid (VOF) method with boundary compressed technique is employed to capture the free surface. The continuity equation and incompressible Navier-Stokes equations with a laminar model are chosen as the governing equations.

$$\nabla \cdot \mathbf{U} = 0 \tag{1}$$

$$\frac{\partial(\rho \mathbf{U})}{\partial t} + \nabla \cdot \left(\rho(\mathbf{U} - \mathbf{U}_g)\right)\mathbf{U} = -\nabla p_d - \mathbf{g} \cdot x \nabla \rho + \nabla \cdot (\mu \nabla \mathbf{U}) + (\nabla \mathbf{U}) \cdot \nabla \mu + \boldsymbol{f}_\sigma \tag{2}$$

Where $\mathbf{U}$ is the flow velocity, $\mathbf{U}_g$ is the speed of mesh grid, induced by the dynamic mesh. ρ denotes the mixture density of the air phase and water phase. p_d is the dynamic pressure. $\mathbf{g}$ is the gravity acceleration vector. μ is the dynamic viscosity. $\boldsymbol{f}_\sigma$ represents the surface tension term, which only takes effect on the free surface.

2.2 Structure solver

An open-source three-dimensional (3D) FEM code CalculiX [15] is employed in this work to calculate the structure deformation of flexible tube WEC. The weak form of the balance of momentum is used as the governing equation of finite element method [16], which can be written as:

$$\rho_s \frac{D^2 \mathbf{U_s}}{D^2 t^2} = \nabla \cdot \mathbf{P} + \rho_s \mathbf{f} \tag{3}$$

$$\mathbf{P} = \mathbf{C} : \mathbf{E}, \quad \mathbf{E} = \frac{1}{2}(\mathbf{F^T F} - \boldsymbol{\delta}) \tag{4}$$

Where ρ_s is the density of the structure. $\mathbf{U_s}$ is the displacement vector of the structure. $\mathbf{P}$ is the second Piola–Kirchoff stress tensor, which is used to calculate the surface force. $\mathbf{f}$ denotes the body force of pre-unit mass, such as the gravity force. $\mathbf{C}$ represents the elasticity tensor, $\mathbf{E}$ denotes the Green–Lagrange strain tensor. $\mathbf{F}$ is the deformation gradient, $\boldsymbol{\delta}$ is the unit tensor.

In CalculiX, the nonlinear behaviour of flexible material can be modelled by using hyper-elastic model, which is described by the following strain energy potential equation [17]:

$$E = \sum_{i=1}^{N} C_{i0}(\bar{I}_1 - 3)^i + \sum_{i=1}^{N} \frac{1}{D_i}(J - 3)^{2i} \tag{5}$$

Where I_1 denotes the Cauchy-Green deformation tensors, C_i and D_i are constants, determined by the material test results.

2.3 Fluid-structure coupling

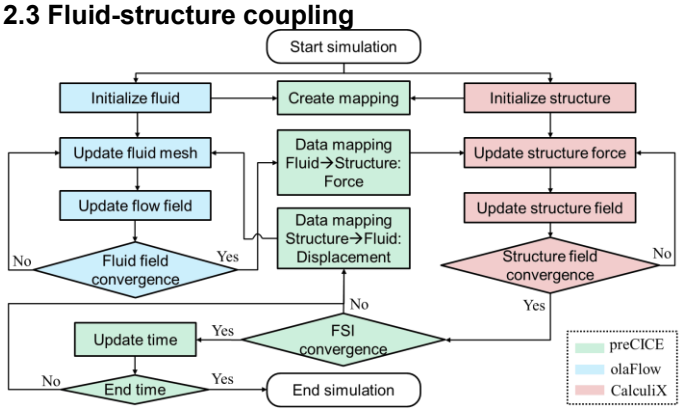

FIGURE 1: SOLVING PROCEDURE OF FSI SIMULATION FOR FLEXIBLE TUBE WEC.

To tackle the interaction of fluid and structure, the multi-physical coupling library pre-CICE is employed [18] to achieve a strong coupling between the structure and fluid solvers. The adaptors used to connect CalculiX and olaFlow with preCICE have been implemented by Uekermann et al. [19] and Gerasimos

[20], respectively. An implicit scheme is used here to ensure numerical stability and convergence, and an improved IQN-IL method [21] is applied to accelerate the coupling iterations. In addition, an interpolation approach [22] based on radial basis functions (RBF) is implemented to transfer the node force from the fluid to the solid and vertices displacements oppositely. The solving procedure of FSI simulation for flexible tube WEC is presented in Figure 1.

3. PROBLEM DESCRIPTION

3.1 Anaconda WEC model

The Anaconda WEC model, shown in Figure 2, is composed of a flexible horizontal tube, a rigid elbow and a rigid vertical tube. An orifice plate is placed on the top of the vertical tube to account for the impedance of PTO. The tube is filled with water, and the initial water elevation in the vertical tube is set to be 0.15m above the external free surface, providing an excess pressure of 1500Pa in the flexible tube. The geometry dimensions of the model can be found in Figure 2.

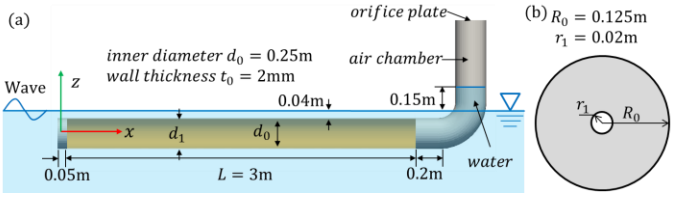

FIGURE 2: SCHEMATICAL DIAGRAM OF THE ANACONDA MODEL (NOT TO SCALE): (a) FRONT VIEW; (b) ORIFICE PLATE.

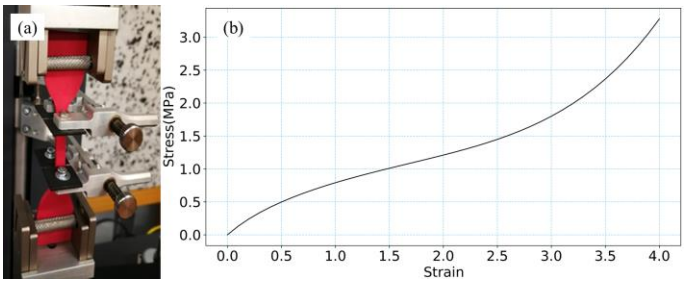

FIGURE 3: (a)SETUP FOR UNIAXIAL TESTS OF THE NATURAL RUBBER; (b) FITTED STRESS-STRAIN CURVE OF NATURAL RUBBER.

TABLE 1: HYPER-ELASTIC CONSTANTS NATURAL RUBBER IMPLEMENTING YEOH MODEL.

YEOH - Reduced Polynomial N3		
C_{10} (MPa)	C_{20} (MPa)	C_{30} (MPa)
0.240	-4.142E-03	1.827E-04

For this analysis, the flexible tube is made of a premium Natural Rubber provided by the company Coruba UK that boasts outstanding strength, resilience and excellent resistance to cuts, tears and abrasion wear is considered. The material was characterised under uniaxial loading conditions using a computer-controlled Testomestric 500X-50 type universal servo-electric test machine, as shown in Figure 3(a). At least five samples are evaluated to verify the repeatability of the properties and a long travel extensometer is used to measure the deformation. With the aim to reproduce the material response in the numerical model, hyper-elastic constants are obtained by implementing YEOH model in ABAQUS with strain energy potential order 3 and considering an incompressible material. Table 1 summarises the YEOH hyper-elastic constants used in the numerical model. The fitted strain-stress curve of Natural Rubber is presented in Figure 3(b).

3.2 Bulge wave speed

According to the linear theory described in Lighthill's study [5], the bulge wave speed of a homogeneous tube is a function of the water density ρ and the distensibility D_t, namely

$$C_b = 1/\sqrt{\rho D_t} \quad (6)$$

$$D_t = \frac{1}{S}\frac{\partial S}{\partial p} \quad (7)$$

Where S is the cross-sectional area, p is the excess pressure.

To obtain the bulge wave speed of the flexible tube, the pressure is measured as well as the cross-sectional area at different positions (x/L =0.12,0.25,0.38,0.5,0.62,0.75,0.88). Figure 4 plots the time histories of these variables. Based on Equation (7), the D_t of the flexible tube at different positions is calculated, and the estimated distensibility values are almost the same, about $6.76\times 10^{-5}\mathrm{ms^2/kg}$, indicating that the results are reasonable. The corresponding bulge wave speed C_b is 3.8m/s when water density ρ is set to $1025\mathrm{kg/m^3}$.

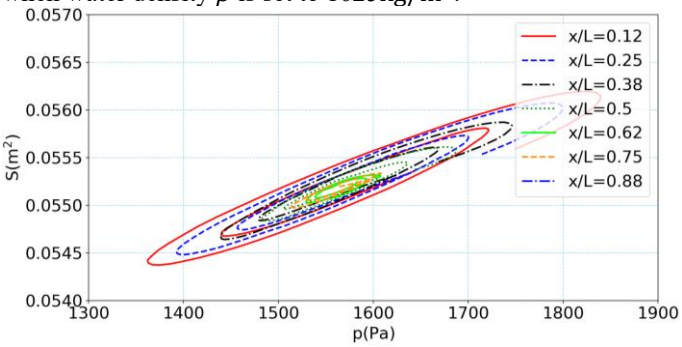

FIGURE 4: INTERNAL PRESSURE VERSUS CROSS-SECTIONAL AREA.

3.3 Wave condition

TABLE 2: WAVE CONDITIONS.

No.	Wave period T_w(s)	Wave speed C_g(m/s)	Wavelength L_w(m)	C_g/C_b
Case 1	1.4	2.19	3.06	0.58
Case 2	1.9	2.97	5.64	0.78
Case 3	2.45	3.82	9.35	1.01
Case 4	2.9	4.46	12.93	1.17
Case 5	3.4	5.0	17.15	1.32

According to Farley and Rainey's study [23], there will be a resonant transfer of energy to the tube when the bulge wave in the tube is the same as the velocity of the waves in the sea. It means that resonant responses occur when the bulge wave speed (C_b) matches the phase velocity (C_g) of the incident wave. In the present work, Stocks 2nd order regular wave is chosen as the

incident wave. To observe the resonant responses of the WEC, we set a series of wave conditions, summarised in Table 2. The ratio of incident wave speed to bulge wave speed (C_g/C_b) varies from 0.58 to 1.32, while the wave amplitude (a) in all cases is kept at 0.03m.

3.4 Grid and time step convergence tests

A cuboid region of 5.6m×2m×3.07m is generated as the computational domain for the numerical simulation. As shown in Figure 5, the Anaconda WEC model is aligned in the direction of wave travel. The water depth is 1.87m, and the height of the air-phase is 1.2m. The model is placed in the centre of the computational domain, and the distances from the inlet and outlet boundaries to the model are both 1m.

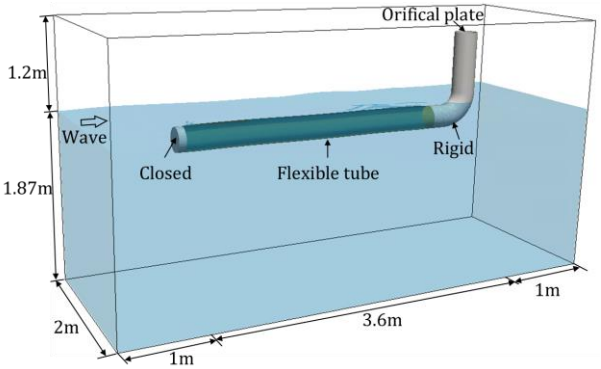

FIGURE 5: COMPUTATION DOMAIN (NOT TO SCALE).

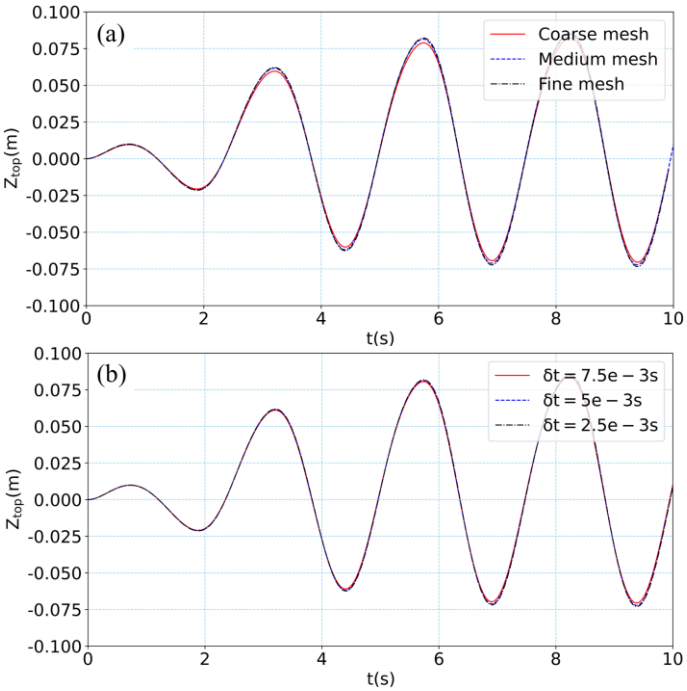

FIGURE 6: TIME HISTORY OF FLEXIBLE TUBE DEFORMATION AT THE TOP POINT OF X/L=0.5 SECTION WITH DIFFERENT: (a) MESH SIZE; (b) TIME STEP.

Convergence tests are carried out to determine the appropriate grid size and the time step for the numerical simulation, where the wave condition is the Case 3 in Table 2. Figure 6 shows the time history of the flexible tube deformation (Z_{top}) at the top point of x/L =0.5 section with different grid sizes and time steps. The surface mesh size of the medium mesh is 1.67% of the tube length (L=3m), which is 2.5% and 0.83% for coarse mesh and fine mesh. It can be seen from Figure 6(a) that the results predicted by medium mesh and fine mesh are very close to each other, thus the medium mesh is chosen to reduce the computational cost. Regarding the time step, indicated by Figure 6(b), the deformation under the time step (δt) of 5e-3s is closer to that under the time step of 2.5e-3s. Therefore, a time step of 5e-3s is set for the next numerical simulations. In this study, the parallel run was performed by two Cirrus [24] standard compute nodes that contain two 2.1 GHz, 18-core Intel Xeon E5-2695 (Broadwell) series processors. The simulation approximately took 26 seconds to completely run one time step. The total elapsed simulation time to obtain the results was approximately 68 hours.

3.5 Verification of code for flexible WEC modelling

To verify the coupled analysis tool, numerical simulations are performed for the Poly-A-OWC model [25], a typical flexible oscillating water column (OWC) WEC. As shown in Figure 7, the top of the collector is covered by a flexible membrane. Two conditions are considered: (a) collector only; (b) collector and membrane. The comparison of the present numerical results and experimental data is plotted in Figure 8. For condition (a), the RAO predicted shows reasonable agreement with the experiment data. However, when considering the flexible membrane in condition (b), the differences between CFD and experiment can be observed. This could be mainly induced by the absence of the pre-stretching of the flexible membrane in the numerical analysis. At present, the current code can only handle a pre-stretching as large as 20% because of its induced highly numerical instability, while in the experiment, the pre-stretching was as large as 250%. Figure 8 also indicates that the measured resonance frequency is larger than the predicted by the numerical method, indicating that pre-stretching increases the natural frequency of the system.

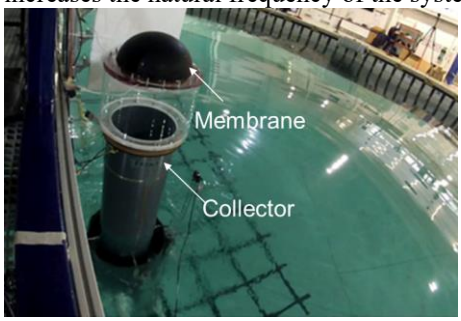

FIGURE 7: POLY-A-OWC MODEL [22].

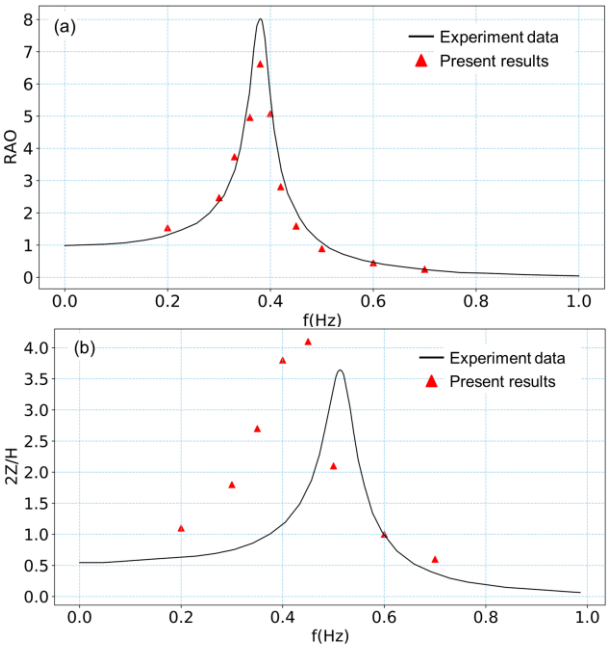

FIGURE 8: COMPARISON OF NUMERICAL RESULTS AND EXPERIMENT DATA: (a) COLLECTOR ONLY; (b) COLLECTOR AND FLEXIBLE MEMBRANE.

4. RESULTS AND DISCUSSIONS

The results will be presented in this section, starting with the wave-structure interaction phenomena, including the observed wave nonlinearity, internal pressure distribution and flow velocity. The impact of incident wave speed on the flow field and capture width is then examined to illustrate the resonant responses of the Anaconda WEC. Moreover, the structure responses of the flexible tube under varying external wave speeds, such as the bulge generation, hoop stress and deformed shape, are also discussed.

4.1 Wave structure interaction

Unlike the linear potential flow theory in the linear numerical models [5, 9], the present tool uses CFD method to model the 3D viscous flow around the WEC, which inherently considers wave nonlinearity induced by the wave-structure interaction. As mentioned earlier, the tube is close to the free surface, thus it easily moves above the free surface and broke the wave shape, leading into a wave nonlinearity, which is observed in the wave tank test [26] and it is very well captured in our numerical results. As shown in Figure 9, the change of wave shape caused by the tube movement is observed. However, for those using linear numerical model, the tube is assumed to be entirely imposed into water all the time. Although the impact of this wave nonlinearity on the Anaconda WEC performance needs to be further explored, the numerical analysis tool in this work is demonstrated to be able to capture the flow details around the WEC.

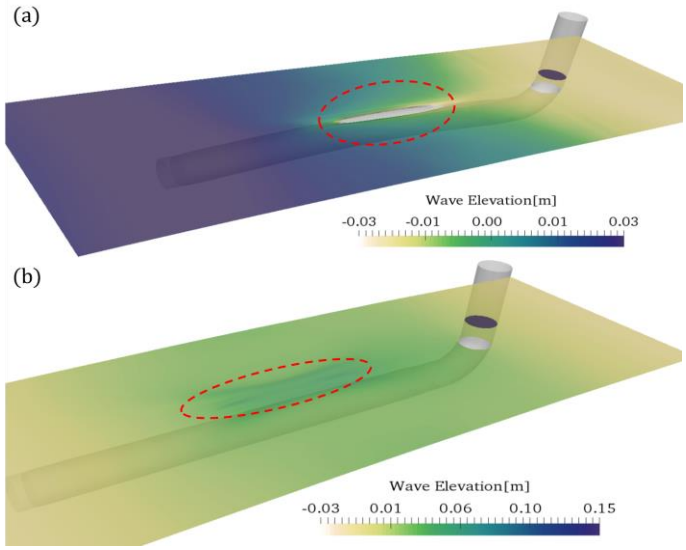

FIGURE 9: INSTANTANEOUS WAVE SURFACE (CASE 3): (a) ABOVE FREE SURFACE; (b) BELOW FREE SURFACE.

To clearly observe the internal flow in the flexible tube, we plot the internal pressure and velocity distribution on the cross-section at different positions (x/L=0.2, 0.4, 0.6, 0.8), as shown in Figure 10. The maximum difference in internal pressure distributed over the tube cross-section within a wave period is 5%, which is 8% for the internal flow velocity. It indicates that the internal pressure and velocity can be considered to be uniformly distributed over the cross-section. This is consistent with the 1D flow assumption in the linear numerical models. Therefore, the pressures and velocities along the centre line of the flexible tube are selected to represent the internal flow field characteristics over the length of the tube, as shown in Figure 11. Due to the external incident wave, the internal pressure and velocity both periodically vary with time, and the internal flow velocity increases with distance along the tube, suggesting that the wave energy is gradually transferred into the internal fluid. The power density reaches its maximum at the end of the tube (x/L=1), where the PTO is usually located. In this work, a rigid orifice plate is placed on the top of the vertical tube to consider the damping of PTO. For comparison, the condition without an orifice plate is also considered. To reflect the impact of the orifice plate on the flow field, we plot the velocity distribution near the orifice plate, as shown in Figure 12. Due to the blocking effect of the orifice plate, the velocity near the hole is accelerated, and a high inhomogeneous distribution of velocity in the air-chamber is also observed.

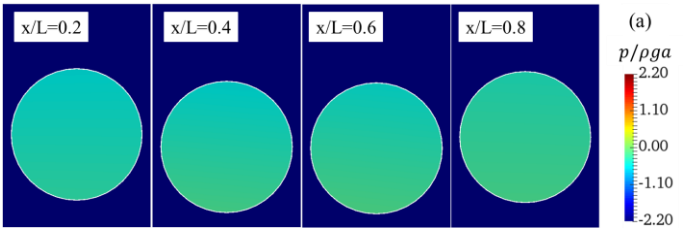

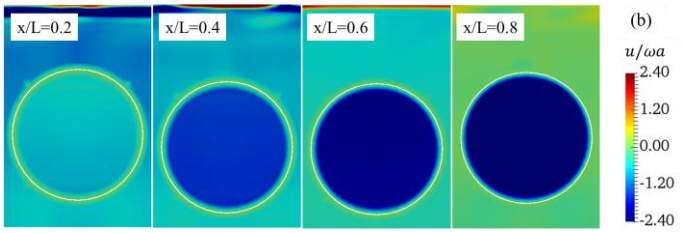

FIGURE 10: INSTANTANEOUS INTERNAL PRESSURE AND VELOCITY DISTRIBUTION ON DIFFERENT CROSS SECTIONS (CASE 3) ALONG THE TUBE: (a) PRESSURE (NORMALIZED BY $\rho g a$); (b) VELOCITY (NORMALIZED BY ωa, $\omega=2\pi/T_w$).

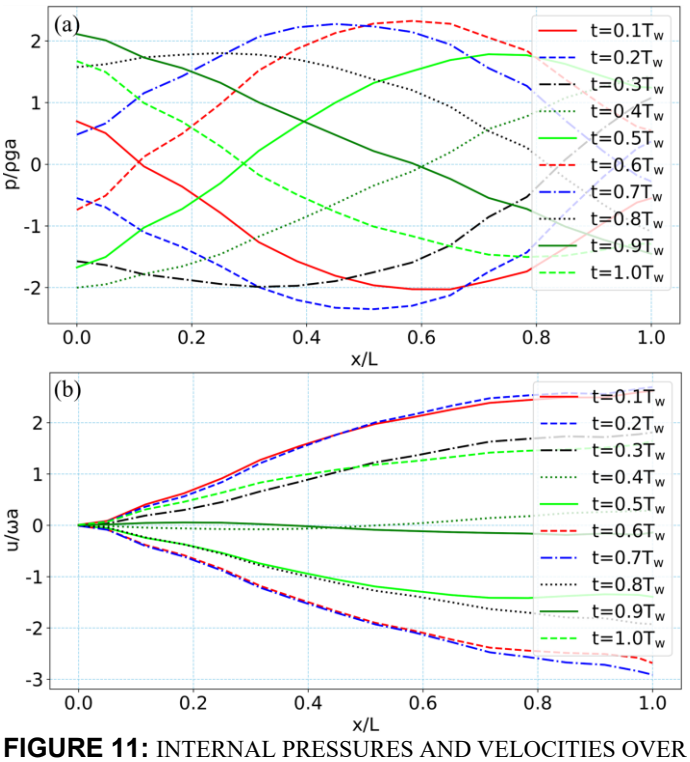

FIGURE 11: INTERNAL PRESSURES AND VELOCITIES OVER THE LENGTH OF THE TUBE AT 10 INSTANTS OVER ONE PERIOD (CASE 3): (a) PRESSURE; (b) VELOCITY.

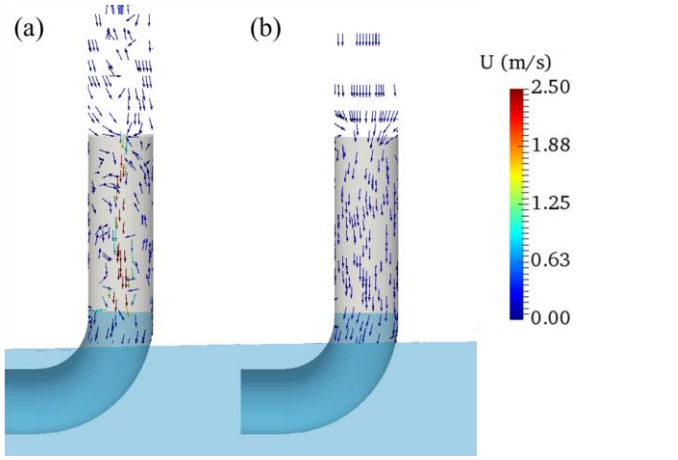

FIGURE 12: INSTANTANEOUS VELOCITY DISTRIBUTION IN THE AIR-CHAMBER ABOVE THE WATER SURFACE: (a) WITH AN ORIFICE PLATE (CASE 3); (b) WITHOUT AN ORIFICE PLATE.

As mentioned earlier, the WEC's PTO usually locates at the tube stern, therefore, the pressures at x/L=1 under different wave conditions are plotted in Figure 13 to investigate the impact of external wave speed on the capture power of WEC. The pressure amplitude reaches its maximum value when the external wave speed matches the bulge wave speed (C_g/C_b=1.01), indicating a typical resonant phenomenon. Affected by the pressure variation at the tube stern, the motion amplitude of the wave column in the vertical tube also shows a peak at resonance (C_g/C_b=1.01), presented in Figure 14. The volume flux across the orifice plate induced by the motion of the water column presented in Figure 15 show a similar trend of pressure variation with internal wave speed, the amplitude of volume flux is also the largest at the resonance condition (C_g/C_b=1.01). To further reflect the impact of external wave speed on the capture power of WEC, the magnitudes of CW under different wave speeds are calculated according to the following equations, and the results are plotted in Figure 16.

$$W = \int_0^{T_w} p(t)Q(t)\mathrm{d}t \tag{8}$$

$$CW = W/\tfrac{1}{2}\rho g a^2 C_g \tag{9}$$

Where p is the pressure at the orifice plate, Q is the volume flux across the orifice plate. The CW is normalized by the tube diameter (D=0.25m), showing a peak value at resonance (C_g/C_b=1.01) as expected.

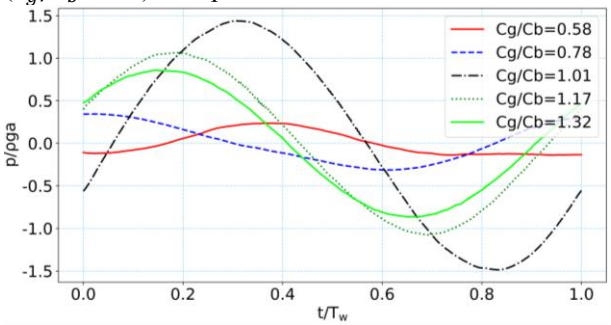

FIGURE 13: TIME HISTORY OF INTERNAL PRESSURE AT THE CENTRE POINT OF CROSS SECTION AT X/L=1.

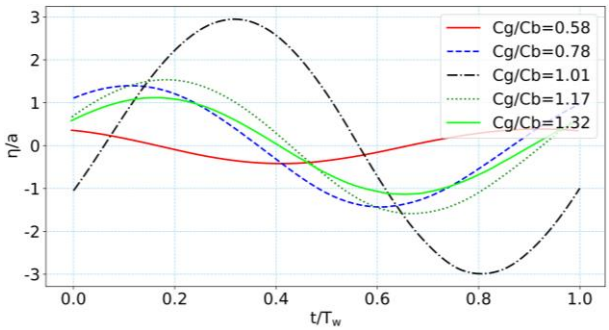

FIGURE 14: TIME HISTORY OF WATER ELEVATION IN THE VERTICAL TUBE.

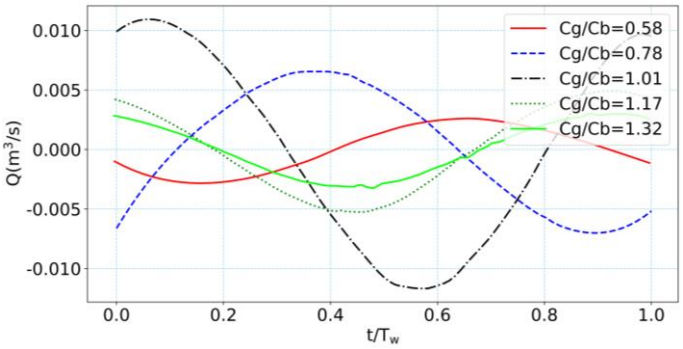

FIGURE 15: TIME HISTORY OF VOLUME FLUX ACROSS THE PLATE.

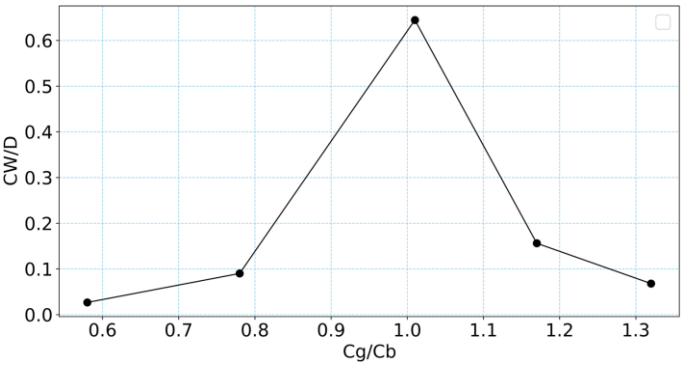

FIGURE 16: CAPTURE WIDTH (NORMALIZED BY THE DIAMETER OF TUBE) VERSUS THE RATIO OF WATER WAVE SPEED TO BULGE WAVE SPEED.

4.2 Flexible tube deformation

Compared with the linearised wall equation adopted by the linear numerical model [9], the 3D FEA approach in this tool is able to better capture the structure deformation and stress distribution characteristics. Figure 17 shows the instantaneous structural deformation and stress distribution on the flexible tube. The deformation along the tube is not uniform, and the maximum deformation occurs near the middle of the tube. The maximum stress appears at both the tube bow and stern, suggesting that these positions have a higher risk of failure, thus more attention should be paid. In addition, the stress distribution in the cross-section, especially at the tube bow and stern, is inhomogeneous, which is unable to capture using the linear numerical model.

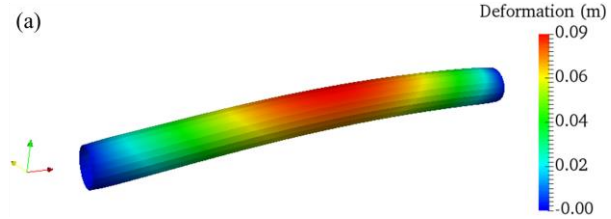

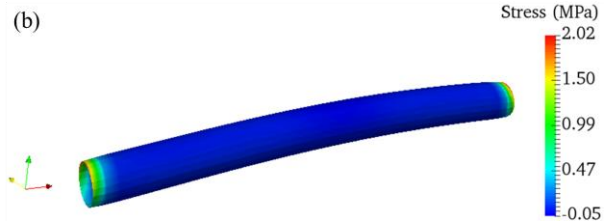

FIGURE 17: INSTANTANEOUS STRUCTURE RESPONSES OF FLEXIBLE TUBE (CASE 3): (a) DEFORMATION; (b) STRESS.

One of the most typical deformation characteristics of the Anaconda WEC is the bulge of the flexible tube, appearing as the cross-sectional area change. To better reflect the bulge of the flexible tube, caused by the internal and external flow, we plot the time and spatial distribution of the cross-sectional area change along the tube length within two wave periods, as shown in Figure 18. As seen, the area varies with a time period closer to the wave period. The influence of external wave speed on the bulge of the flexible tube, plotted in Figure 19, shows the area increases at resonance condition as C_g/C_b=1.01, which further results in a larger hoop stress, as shown in Figure 20.

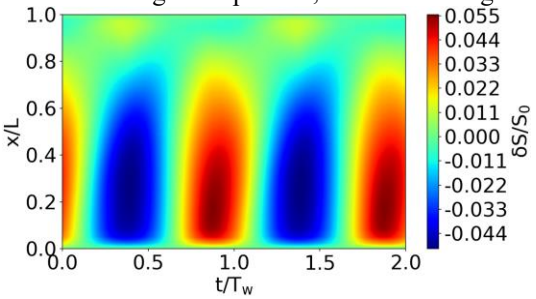

FIGURE 18: TIME AND SPATIAL DISTRIBUTION OF THE CHANGE OF SECTION AREA (CASE 3).

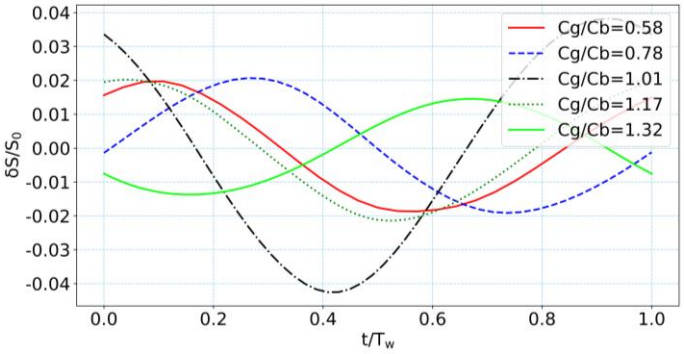

FIGURE 19: TIME HISTORY OF THE CHANGE OF SECTION AREA (NORMALIZED BY INITIAL AREA S_0) AT X/L = 0.5.

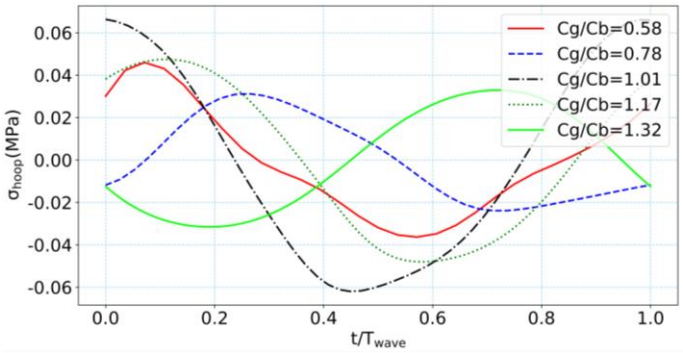

FIGURE 20: TIME HISTORY OF THE HOOP STRESS OF THE CROSS-SECTION AT X/L = 0.5.

Figure 21 presents the envelope of flexible tube deformation for given wave conditions., where d_z is the displacement of the flexible tube along z-axis, and D=0.25m is the initial inner diameter of the flexible tube. It can be found that the ratio of tube length (L) to the wavelength (L_w) has significant impacts on the excited mode of the flexible tube deformation. When $L \approx L_w$, as shown in Figure 21(a), the 2nd dominant mode of the tube is captured. When $L < L_w$, the 1st dominant mode of the tube is observed. In addition, it can be observed that the deformation amplitude of the flexible tube at resonance (C_g/C_b=1.01) is larger than that under the other conditions.

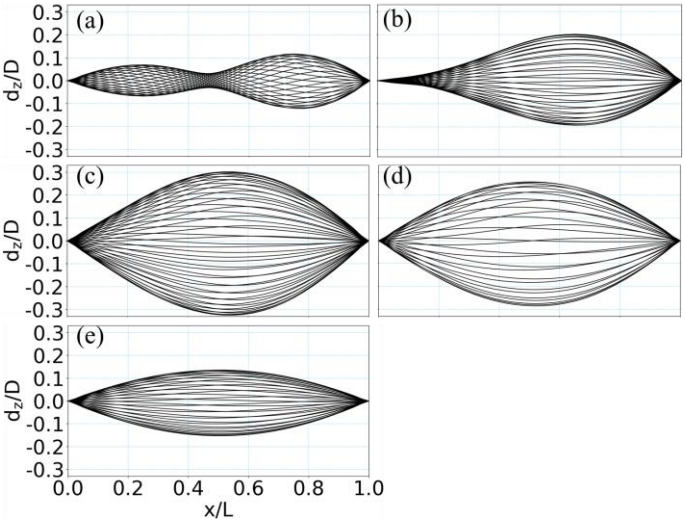

FIGURE 21: SHAPE OF FLEXIBLE TUBE AT DIFFERENT INSTANTS OVER ONE PERIOD: (a) C_g/C_b=0.58; (b) C_g/C_b=0.78; (c) C_g/C_b=1.01; (d) C_g/C_b=1.17; (e) C_g/C_b=1.32.

5. CONCLUSION

In this paper, a coupled numerical analysis tool based on computational fluid dynamics and a finite element method is employed to perform numerical simulations for the Anaconda WEC model consisting of natural rubber under given different regular wave conditions. The nonlinear behaviour of flexible material is taken into account by using YEOH hyper-elastic model. Fluid-structure interaction responses of the Anaconda WEC are compared considering the impact of the external wave speed on the performance of the system.

The results show that the proposed numerical analysis tool is able to predict the complex fluid-structure interaction responses of flexible tube WEC in waves. Compared with the linear numerical model, the present tool can provide more flow details and structure deformation information, especially for the nonlinear responses, such as the wave nonlinearity induced by the tube movement and the inhomogeneous distribution of stress at the cross-section. Typical resonant responses of WEC are also successfully captured when the bulge wave speed matches the incident wave speed. As expected, the internal pressure amplitude, capture width, variation of section area and hoop stress all increase at resonant condition. Moreover, the deformed shape of the flexible tube is found to depend on the ratio of wavelength to tube length. When the wavelength matches the tube length, the dominant mode of the flexible tube is 2nd order, which is decreased to 1st order if the wavelength is larger than the tube length.

The present work contributes to the study of fluid-structure interaction responses of flexible tube WEC for regular waves. However, limited by the code development, the 6DoF motions of the WEC is not taken into account in this study, which is our near future work.

ACKNOWLEDGEMENTS

This research was supported by an EPSRC Grant “Bionic Adaptive Stretchable Materials for WEC (BASM-WEC)” (No. EP/V040553/1). This work used the Cirrus UK National Tier-2 HPC Service at EPCC (http://cirrus.ac.uk) funded by the University of Edinburgh and EPSRC (EP/P020267/1).

REFERENCES

[1] Moretti G, Herran M S, Forehand D, Alves M, Jeffrey H, Vertechy R, Fontana M. Advances in the development of dielectric elastomer generators for wave energy conversion[J]. Renewable and Sustainable Energy Reviews, 2020, 117: 109430.

[2] Jean P, Wattez A, Ardoise G, Melis C, Van Kessel R, Fourmon A, Barrabino E, Heemskerk J, Queau J P. Standing wave tube electro active polymer wave energy converter[C]//Electroactive Polymer Actuators and Devices (EAPAD) 2012. SPIE, 2012, 8340: 75-95.

[3] Heller V, Chaplin J R, Farley F J M, Hann M R, Hearn G E. Physical model tests of the anaconda wave energy converter[C]//Proc. 1st IAHR European Congress. 2000.

[4] Farley F J M D, Rainey R C T. Distensible tube wave energy converter: U.S. Patent 7,980,071[P]. 2011-7-19.

[5] Lighthill M J, Lighthill J. Waves in fluids[M]. Cambridge university press, 1978.

[6] Chaplin J R, Heller V, Farley F J M, Hearn G E, Rainey, R C T. Laboratory testing the Anaconda[J]. Philosophical Transactions of the Royal Society A: Mathematical, Physical and Engineering Sciences, 2012, 370(1959): 403-424.

[7] Mendes A C, Braga F P, Paredes L M A, Chaplin J R. Performance assessment of the ANACONDA WEC in regular waves at 1: 50 model scale[C]//International Conference on Offshore Mechanics and Arctic Engineering. American Society of Mechanical Engineers, 2017, 57786: V010T09A016.

[8] Checkmate Flexible Engineering, https://www.checkmateukseaenergy.com/, accessed 15th December 2022.

[9] Babarit A, Singh J, Mélis C, Wattez A, & Jean P. A linear numerical model for analysing the hydroelastic response of a flexible electroactive wave energy converter[J]. Journal of Fluids and Structures, 2017, 74: 356-384.

[10] Chaplin J R, Farley F J M, Hearn G E, Heller V, Mendes A. Hydrodynamic performance of the anaconda wavepower device[C]//Proc. Of the HYDRALAB III Joint User Meeting, Hannover. 2010.

[11] Chaplin J R, Farley F J M, Prentice M E, Rainey R C T, Rimmer S J, Roach A T. Development of the ANACONDA all-rubber WEC[J]. 2007.

[12] Li X, Xiao Q. A numerical study on an oscillating water column wave energy converter with hyper-elastic material[J]. Energies, 2022, 15(22): 8345.

[13] Higuera P, Lara J L, Losada I J. Three-dimensional interaction of waves and porous coastal structures using OpenFOAM®. Part I: Formulation and validation[J]. Coastal Engineering, 2014, 83: 243-258.

[14] Higuera P, Lara J L, Losada I J. Three-dimensional interaction of waves and porous coastal structures using OpenFOAM®. Part II: Application[J]. Coastal Engineering, 2014, 83: 259-270.

[15] Dhondt G. Calculix crunchix user's manual version 2.12[J]. Munich, Germany, accessed September 2017, 21: 2017.

[16] Luo Y, Xiao Q, Shi G, Wen L, Chen D, Pan G. A fluid–structure interaction solver for the study on a passively deformed fish fin with non-uniformly distributed stiffness[J]. Journal of Fluids and Structures, 2020, 92: 102778.

[17] Martins P, Natal Jorge R M, Ferreira A J M. A comparative study of several material models for prediction of hyperelastic properties: Application to silicone-rubber and soft tissues[J]. Strain, 2006, 42(3): 135-147.

[18] Bungartz H J, Lindner F, Gatzhammer B, Mehl M, Scheufele K, Shukaev A, Uekermann B. preCICE–a fully parallel library for multi-physics surface coupling[J]. Computers & Fluids, 2016, 141: 250-258.

[19] Uekermann B, Bungartz H J, Yau L C, Chourdakis G, Rusch A. Official preCICE adapters for standard open-source solvers[C]//Proceedings of the 7th GACM colloquium on computational mechanics for young scientists from academia. 2017.

[20] Chourdakis G. A general OpenFOAM adapter for the coupling library preCICE[J]. 2017.

[21] Degroote J, Bathe K J, Vierendeels J. Performance of a new partitioned procedure versus a monolithic procedure in fluid–structure interaction[J]. Computers & Structures, 2009, 87(11-12): 793-801.

[22] Lindner F, Mehl M, Uekermann B. Radial basis function interpolation for black-box multi-physics simulations[J]. 2017.

[23] Farley F J M, Rainey R C T. Radical design options for wave-profiling wave energy converters[J]. IWWWFB06, 2006.

[24] Cirrus, https://www.cirrus.ac.uk/about/hardware.html, accessed 16th February 2023.

[25] Moretti G, Rosati Papini G P, Daniele L, Forehand D, Ingram D, Vertechy R, Fontana M. Modelling and testing of a wave energy converter based on dielectric elastomer generators[J]. Proceedings of the Royal Society A, 2019, 475(2222): 20180566.

[26] Farley F J M, Rainey R C T, Chaplin J R. Rubber tubes in the sea[J]. Philosophical Transactions of the Royal Society A: Mathematical, Physical and Engineering Sciences, 2012, 370(1959): 381-402.